Efficiency Improvement by Deriving the Optimal Operating Slip Frequency of a Linear-Induction-Style Maglev Train

Sang-Uk Park [1], Hyung-Soo Mok [1], Jae-Won Lim [2], Hyun-Uk Seo [3] and Sang-Hun Oh [1,*

[1]   Department of Electrical Engineering, Konkuk University, Seoul 05029, Korea;
     shyman01@konkuk.ac.kr (S.-U.P.); hsmok@konkuk.ac.kr (H.-S.M.)
[2]   Department of AI Machinery, System Engineering Research Division, Korea Institute of Machinery and
     Materials, Daejeon 34103, Korea; einses@kimm.re.kr
[3]   Department of Robotics & Mechatronics, Korea Institute of Machinery and Materials, Daejeon 34103, Korea;
     shu@kimm.re.kr
*   Correspondence: osh@muha.kr

Abstract: While urban maglev trains have the advantage of being optimized for urban environments where noise is low and dust is less generated, their driving efficiency is low when compared to rotary induction motors owing to the structural limitations of linear devices. To compensate for these disadvantages, various studies on train control schemes have been conducted. Representative control methods include improving the efficiency of using slip frequency by directly controlling the propulsion force using vector control. However, this method has limitations in its use as it relates to the normal force that affects the train's levitation system. Therefore, in this study, mathematical analysis was conducted for each factor that mutually affects the control of the train. On this basis, the magnitude of the normal force related to the safety of the train is limited. Operating efficiency was improved by varying the slip frequency according to the operating conditions of the train. In addition, for verification, the effect was proved through a comparative experiment using an 18 ton class maglev train running at Incheon International Airport.

1. Introduction

The linear induction motor (LIM) has been widely studied as a transportation system running in urban areas owing to its low noise, environmentally friendly factors that do not generate dust, and its excellent performance on slopes and around sharp curves. An LIM is a system that levitates and is propelled through the interaction of the rails and vehicles using the power of an electromagnet. It comprises, primarily, a levitation system and a propulsion system. In the levitation system, as shown in Figure 1b, the train guide generates an attraction force through the lower part of the rail to levitate the train. As shown in Figure 1a, the propulsion system generates magnetic flux using an electromagnet mounted on the train, linking it to the rail. Subsequently, the linkage magnetic flux generates a counteracting flux in the direction of the train on the rail. Consequently, the train and rail are attracted and repelled by the correlation between the magnetic flux generated by the electromagnet mounted on the train and the counteracting magnetic flux of the rail. The LIM generate thrust for propulsion through attraction and repulsion—a normal force being generated in the rail direction. Therefore, to generate the thrust required to propel the train, a normal force that does not contribute to the propulsion of the train is generated. In addition, because the normal force is generated in the opposite direction of the levitation force of the train, the levitation system must overcome gravity and normal

forces, and float the train. In other words, the unnecessarily generated normal force is a factor that destabilizes the levitation system of the train, it being a potential safety problem due to train levitation failure. It also induces additional energy consumption in both the propulsion system and the levitation system, thereby reducing efficiency [1]. Therefore, for the efficient operation of trains, a train control technique that reflects the characteristics of linear devices is required.
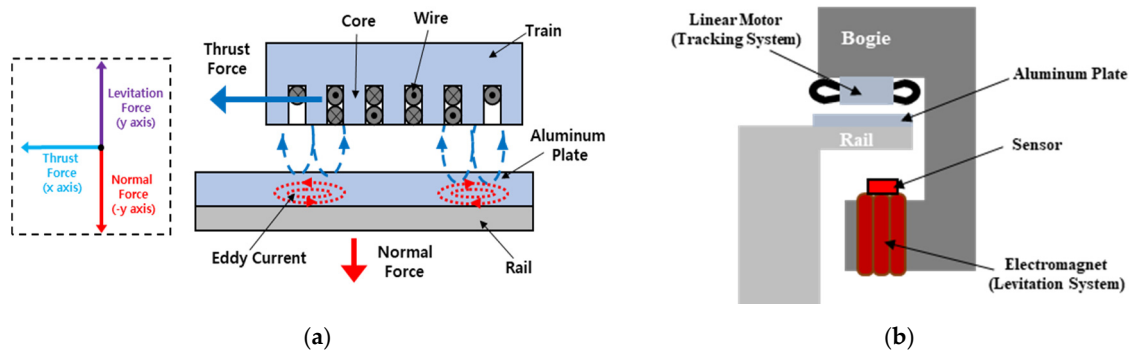

(a)   (b)

Figure 1. Structure of maglev train: (**a**) Structure of trains and rails and (**b**) Structure of levitation system.

For LIM control, a control method using slip frequency and a method using indirect vector control were widely studied. The slip-frequency control method was used because of its independence from parameter fluctuations and ease of implementation. Because the linear motor is based on an induction motor, the size of final load R_L fluctuated according to slip, as shown in Figure 2a. Accordingly, the ratio of the current for magnetization and the current for propulsion fluctuated. As shown in Figure 2b, the magnitude of the input current required for operation based on the slip increased when the slip was large, and decreased when the slip was small [2–5].
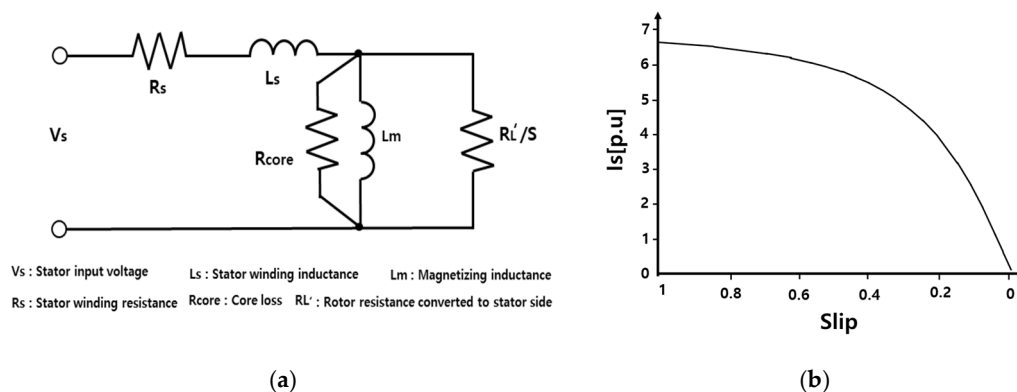

(a)   (b)

Figure 2. Efficiency fluctuation due to slip: (**a**) Induced motor equivalent circuit and (**b**) Input current and slip.

Because the LIM is a system based on an induction motor that cannot directly control the slip, the slip frequency (having a proportional relationship to the slip) was used. Accordingly, a study was conducted on a method of improving efficiency through the size of the slip frequency [6–8]. However, slip is a factor related to the normal force that affects the potential failure of the train. There is also a problem in that normal force increases when the size of slip frequency decreases [9].

In [8], a fixed slip-frequency control method was proposed that used fixed high slip frequency that did not fail to levitate the train. However, by using the same slip frequency in the operating bands of all trains, a problem occurred in that operating efficiency was lowered by using the same slip frequency, even in sections where high slip frequency was not required (on the basis of train operating conditions). Subsequently, a study of a variable slip-frequency control method was conducted to change the slip

frequency on the basis of the operating conditions of the train to lower the slip frequency while limiting the normal force of the LIM [10].

Second, as a method, an indirect vector control method was proposed that is widely used in rotary induction motors with fast response and excellent performance [11]. However, for indirect vector control, the air-gap magnetic flux must be kept constant, but is difficult to apply in the LIM because the air-gap magnetic flux fluctuates during train operation owing to the characteristics of linear devices. In [12–15], a method was presented using the current of the *d* axis, which is the axis where the magnetic flux of the motor is generated during the vector control of an induction motor. The attenuated magnetic flux was compensated by controlling *d*-axis current i_d. However, this method also had a problem, in that i_q associated with the thrust force fluctuated to maintain the slip frequency constant when i_d was changed to compensate for the attenuated magnetic flux, as shown in slip angular velocity Equation (1) of indirect vector control (here, i_q means the current in the *q* axis generating torque in the *d-q* axis for vector control):

$$\omega_{sl} = \frac{1}{T_r} + \frac{i_q}{i_d},$$

(1)

where ω_{sl} is the slip angular velocity, $T_r = \frac{L_r}{R_r}$, L_r is rotor winding impedance, R_r is rotor winding resistance, i_d is the d-axis current (air-gap magnetic flux), and i_q is the q-axis current (thrust).

Accordingly, in [16], a control method using both indirect vector control and variable slip-frequency control was proposed. When the i_d value was changed to compensate for the air-gap magnetic flux, ω_{sl} changed using i_q such that the slip value was within the allowable range. However, because this method was not a result derived through mutual mathematical analysis of train operating conditions, it was difficult to guarantee safety because the exact normal force was unknown. In addition, because all input values for each condition must be derived through direct experiments, the process costs much time and money. For this reason, maglev trains currently in operation utilize a fixed slip-frequency control method that can guarantee train safety. Therefore, in order to improve train efficiency while ensuring safety, it is necessary to analyze the mutual influence through mathematical analysis of the slip, normal force, and propulsion force. On the basis of the analyzed data, if the calculated slip frequency is instantaneously changed on the basis of the operating conditions of the train, it is possible to safely and efficiently operate the train (the proposed method increases efficiency by using the ratio of slip frequency, normal force, and traction force, which are the characteristics of electromagnetic-suspension-type LIM. Therefore, it is difficult to apply this method to types of maglev trains with different structures and driving methods).

The remainder of this paper is organized as follows. In Section 2, the mathematical relationship between normal/propulsion force and slip frequency is analyzed through an investigation of the relationship among normal force, propulsion force, slip, and slip frequency. After that, through the derived equation, the change in efficiency within the limited normal force is presented. Consequently, a control algorithm for controlling the proposed method is presented. In Section 3, the effect is shown through simulation. In Section 4, experimental evaluation conducted using actual vehicles running on the island of Yeongjong, Korea is summarized. Lastly, Section 5 presents our conclusions.

2. Control Method

2.1. Conventional Method

As described above, in a maglev train, both propulsion and normal force fluctuate according to slip. In particular, levitation in the normal force affecting the levitation system of the train becomes a factor that can hinder the safety of the train. Therefore, to control the train, normal force must be controlled by slip. However, because the LIM is a system based on an induction motor and cannot

directly control the slip, it was controlled using slip frequency that has a proportional relationship with the slip, as shown in Equation (2):

$$f_{sl} = f_e S \tag{2}$$

$$f_e = f_m + f_{sl} \tag{3}$$

where f_e is the synchronization frequency, which means the supply frequency of the AC voltage supplied to the stator winding; f_m is the rotor frequency, which is the physical rotation frequency; f_{sl} is the slip frequency, which is the difference between the synchronization frequency and the rotor frequency; and S is the slip, which is the ratio of the slip frequency to the synchronization frequency, and it can be expressed as $s = f_{sl}/f_e$.

Table 1 shows an example of fluctuations in slip and normal force when slip frequency is fixed and the synchronous speed of the train is changed using Equation (2) and Figure 3. Figure 3 shows the normal force value derived through finite-element analysis.

Table 1. Correlation between elements in fixed slip-frequency control.

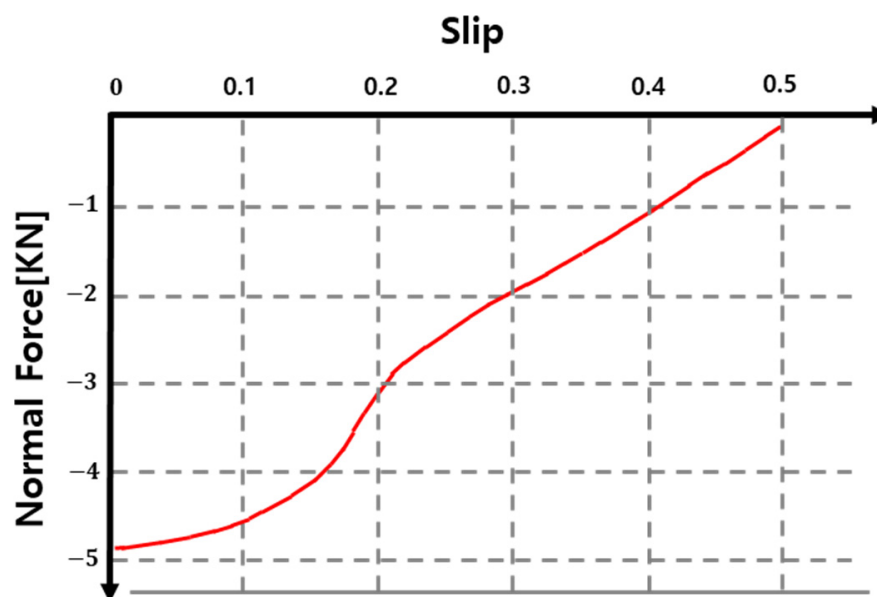| f_{sl} (Hz)	f_e (Hz)	s	Normal Force (N)
	100	0.1	−4500
10	50	0.2	−3000
	33	0.3	−2000

Figure 3. Normal force by slip frequency through finite-element analysis.

Table 1 shows that, as the synchronous frequency associated with the train's synchronous speed decreased, slip increased, maintaining a fixed slip frequency. As shown in Figure 3, as slip increased, vertical force changed in the direction of decreasing, increasing the safety of the train [5,13]. If the slip frequency were fixed, Equation (3) shows that the synchronous speed also had its maximal value at the point where the speed of the train was maximal, and the greatest vertical force occurred at this moment (here, the maximal synchronous speed was the maximal change speed of the magnetic field generated by the stator when the train was running at maximal speed. The greatest normal force was at the moment when the magnitude of the levitation force that made the levitation system unstable was the greatest), that is, if slip magnitude and the normal force at which the levitation did not fail at the maximal speed of the train, maximal slip frequency could be derived from the synchronous speed of the train. If the derived slip frequency were fixed, the train would be in an area where there was less

risk of accidents caused by vertical force when the train is running at full speed. This means that the risk of accidents caused by vertical force would also be low in the section where the speed of the train was decreasing. So, the train could safely run in all speed zones. For train safety, this method is applied to currently running maglev trains. However, this method ignores the train's operating conditions and uses a fixed slip frequency, which leads to low-efficiency train operation due to large slip at low speeds. Consequently, if the ratio of the fluctuations of the propulsion force and normal force of the train based on the slip frequency is known, the efficiency of the train can be improved by adjusting slip frequency within the normal force that operates safety zones according to the required propulsion force.

2.2. Proposed Method

The equations of normal force and levitation force used in the control of a maglev train can be obtained through FEM analysis [17] and the structural properties of the target vehicle. Equations (4) and (5) show the relationship between normal force and slip frequency, and driving force and slip frequency, respectively:

$$F_N = \frac{l\tau\mu_0}{2} \frac{1 - (R_m S)^2}{(sinh\beta g)^2 + (R_m S cosh\beta g)^2} (Z_m I_m)^2 \tag{4}$$

$$F_T = l\tau\mu_0 \frac{R_m S}{(sinh\beta g)^2 + (R_m S cosh\beta g)^2} (Z_m I_m)^2 \tag{5}$$

where $R_m = \sigma_t \mu_0 \lambda f$ is the magnetic Reynolds number, $\sigma_t = \sigma t_{eff}$ is the effective conductivity, t_{eff} is the effective thickness of the secondary conductor, $\beta = \frac{\pi}{\tau}$ is the air:gap:wavelength ratio, $S = 1 - \frac{V_m}{V_{sy}} = \frac{f_{sl}}{f}$ is the slip, V_m is a variable representing the speed of the train, V_{sy} is a variable representing synchronous speed, Z_m is maximal winding density (the maximal winding density per unit length of the train core), I_m is the maximal current (the maximal current input for the required current to operate the system), g is the effective void, τ is the pole spacing, f is the power frequency, σ is the conductivity of the secondary conductor, f_{sl} is the slip frequency, and l is the primary core width.

By deriving the relational expression between driving force and normal force from the relational expressions in Equations (4) and (5), the ratio of normal force and driving force, as shown in Equation (6), can be derived using the equation related to slip frequency:

$$\frac{F_N}{F_T} = -\frac{1}{2}\left(R_m S - \frac{1}{R_m S}\right) \tag{6}$$

where $R_m = \sigma_t \mu_0 \lambda f$ and $S = \frac{f_{sl}}{f}$. From this result, $R_m S$ is slip frequency.

If this is summarized in terms of slip frequency, it can be expressed as Equations (7) and (8). Through Equation (8), the maximal normal force can be obtained from the currently running fixed slip-frequency value. If this maximal normal force is then substituted for the required thrust, the maximal usable slip frequency range can be calculated for each operating condition. That is, if the normal force and the propulsion force at the maximal propulsion force of a currently running train are substituted, slip frequency can be determined and controlled so as to be limited to a range that does not fail in levitation.

$$0 = (\sigma_t \mu_0 \lambda)^2 f_{sl}^2 + 2\frac{F_N}{F_T}(\sigma_t \mu_0 \lambda) f_{sl} - 1 \tag{7}$$

$$f_{sl} = \frac{-2\frac{F_N}{F_T}\sigma_t \mu_0 \lambda \pm \sqrt{(2\frac{F_N}{F_T}\sigma_t \mu_0 \lambda)^2 + 4(\sigma_t \mu_0 \lambda)^2}}{2(\sigma_t \mu_0 \lambda)^2} \tag{8}$$

Figure 4 shows the ratio of normal force/thrust force according to slip frequency using Equation (6). Table 2 uses Figure 4 and Equation (8) to calculate the slip frequency in which the maximal normal force is generated within the range of levitation not failing when propulsion force is changed (if slip

frequency is negative, it operates as a braking mode; if it is positive, it operates as a powering mode for thrust).
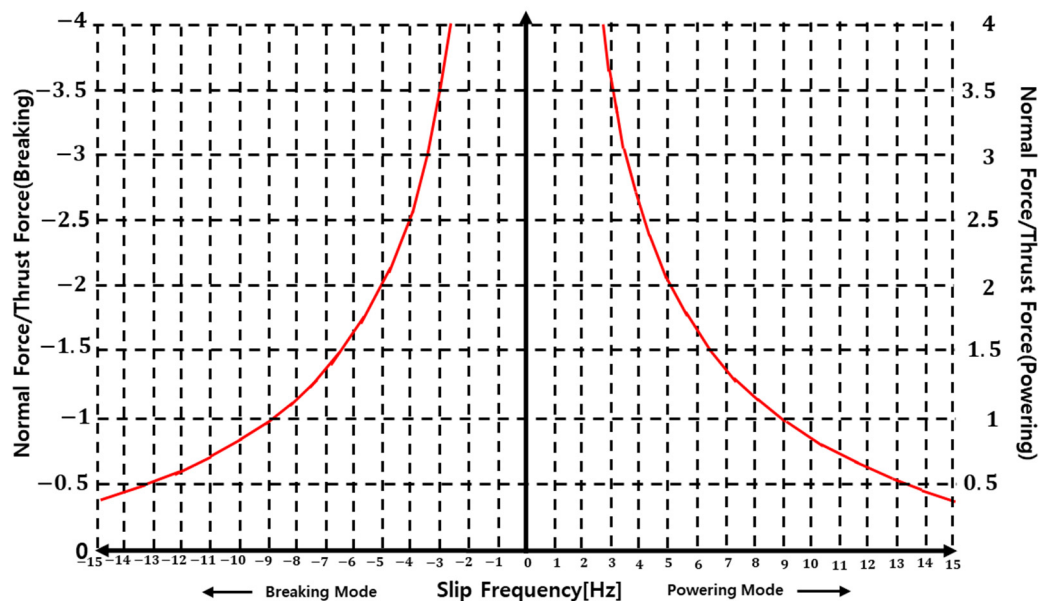

Figure 4. Ratio of normal force and thrust force according to slip frequency.

Table 2. Normal force margin ratio by slip frequency at each thrust.

Thrust	Margin	Slip Frequency (Hz)
100%	1	13.5
75%	1.33	12.5
50%	2	9
30%	3.33	6.5

Table 2 shows that, when the maximal driving force was 100%, when the driving force decreased, the normal force also decreased. Therefore, when using the same slip frequency of 13.5 Hz at approximately 75%, 50%, and 30% thrust, the amount of normal force generated on the basis of maximal thrust is reduced. Assuming that the margin ratio of the normal force is 1 at a slip frequency of 13.5 Hz, margin rates at each operating condition are 1.33, 2, and 3.33, respectively. If slip frequency was lowered by this margin factor, efficient operation would be possible within the range of normal force that did not affect safety. If the optimal slip frequency suitable for train operation conditions were derived in this way, a train-operation pattern capable of varying the appropriate slip frequency during train operation could be obtained.

2.3. Algorithm

Figure 5 shows a block diagram of the proposed control algorithm. Looking at the left side of Figure 5, given thrust command F_T^* and train speed v_m, the recommendation calculator determines the slip-frequency command that can be used within the range not exceeding the normal force limit through the previously proposed method.
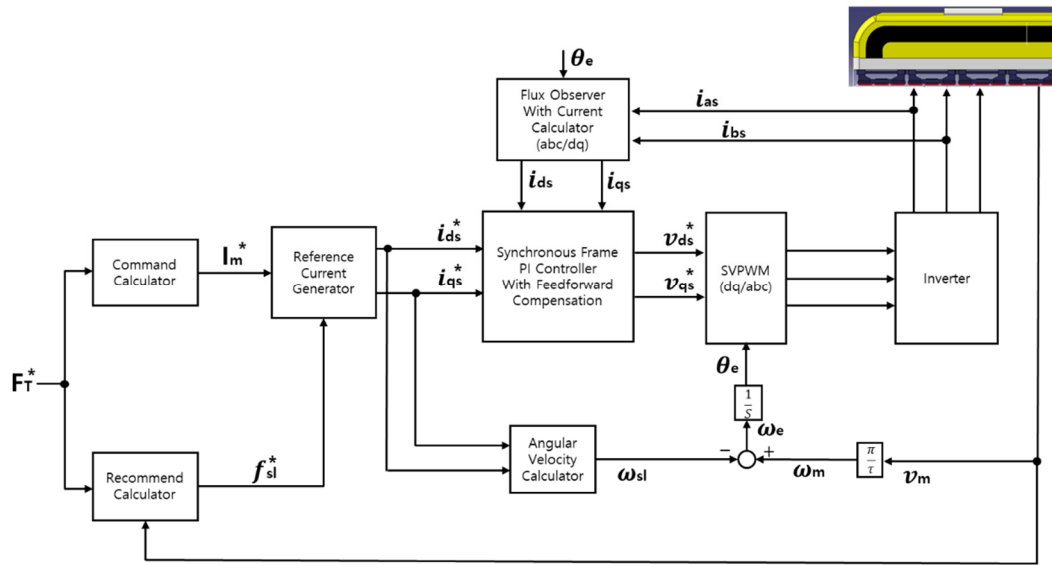
Figure 5. Control algorithm of proposed method.

At this time, the normal force-limit value was derived from finite-element analysis and the initial train test. If derived slip-frequency command f_{sl}^* and command I_m^* of the total current required to drive the system are given as "reference current generator", i_d and i_q for vector control are derived. At this time, total current command I_m^* is determined through Equation (5), and the method of deriving i_d and i_q using "reference current generator" is as follows.

$$\omega_{sl} = \frac{R_r}{L_r} \frac{i_q}{i_d} \tag{9}$$

$$I_{rms}^2 = i_d^2 + i_q^2 \tag{10}$$

Equation (9) shows the relationship between slip frequency and *d-q* axis reference currents i_d and i_q in the induction motor, and Equation (10) shows the relationship between I_m and i_d, i_q derived through the propulsion force. These two equations are used to determine the i_d, i_q current command in the "reference current generator".

$$i_d = \frac{R_r}{L_r} \frac{i_q}{\omega_{sl}} \tag{11}$$

$$I_{rms}^2 = (\frac{R_r}{L_r})^2 (\frac{i_q}{\omega_{sl}})^2 + i_q^2 \tag{12}$$

If Equation (9) is summarized for i_d as in Equation (11) and substituted into Equation (10), Equation (12) representing the relationship between i_q and I_m can be obtained. Reorganizing this for i_q can be expressed as Equation (13):

$$i_q = \frac{L_r}{R_r} \omega_{sl} \sqrt{\frac{1}{(1 + (\frac{L_r}{R_r}\omega_{sl}))^2}} I_{rms} \tag{13}$$

$$i_d = \sqrt{\frac{1}{(1 + (\frac{L_r}{R_r}\omega_{sl}))^2}} I_{rms} \tag{14}$$

By arranging i_d in the same way, we can obtain Equation (14). The current command of the *d-q* axis can be derived from constants R_r and L_r of the train, total current I_m required by the driving force, and slip angular velocity ω_{sl} that can be obtained from the slip frequency. Therefore, when the thrust

and normal force-limit values, which are the driving conditions of the train, are proposed, it is possible to directly control the i_q current, involved in the propulsive force of the train, and i_d, involved in the lift of the train.

3. Simulation

In order to perform the simulation under the same conditions as those of the actual train, the data of a train that was actually operated were used as input values, as shown in Figure 6a, through which the current command and slip required for control of the slip frequency was derived and utilized. The black waveform represents the speed pattern of the train, and the blue waveform represents the driving-force waveform of the train. For efficiency comparison, total power consumption and generated normal force were compared between the conventional method using a slip frequency of 13.5 Hz, and the proposed method in which the slip frequency fluctuated during train operation based on the operating conditions. In the proposed method, the margin rate of the limited normal force was set to vary between 9.5 and 13.5 Hz according to the applied operating conditions.
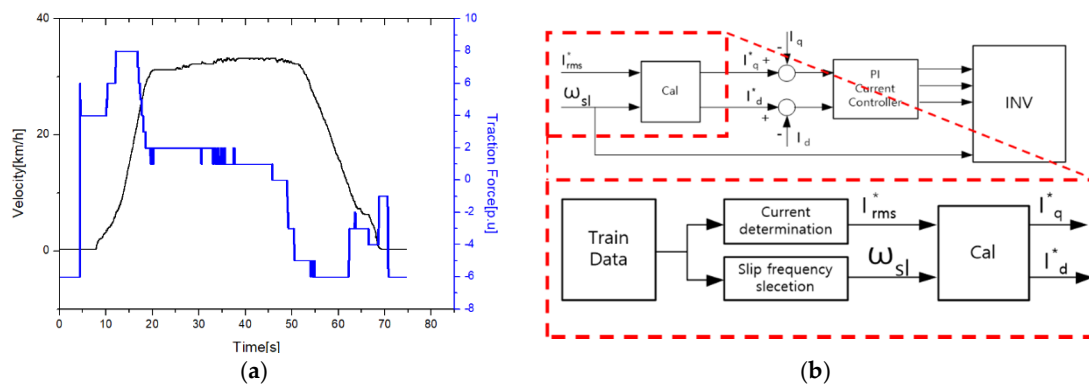

Figure 6. Simulation conditions and calculation blocks: (**a**) Train operation pattern (train data) and (**b**) Block diagram using train pattern.

Figure 7 compares the results of the existing control method and the proposed method. Figure 7a shows the accumulated power consumption while the train was running. The existing control method of the red curve consumed approximately 140 Wh of power while operating under the same conditions and section, whereas the proposed method of the black curve consumed approximately 116 Wh of power, an improvement of approximately 24 Wh, which is a reduction in power consumption and an efficiency improvement of approximately 19.6%. Figure 7b shows the normal force change during train operation. When a margin ratio of approximately 30% was compensated for safety from the actual train's limited normal force, the limit value was about −2.5 kN, called the critical normal force. If the normal force falls below this value, levitation fails. Looking at the waveform in Figure 7b, the maximal generated normal force of the conventional method was −2.04 kN, and the maximal generated normal force of the proposed method was −2.45 kN. Both systems were in the safe area. Therefore, when using the proposed method, efficiency increased by approximately 17.14%, but it was confirmed that the efficiency improvement of the proposed method was effective because the train was running within a safe range of normal force.
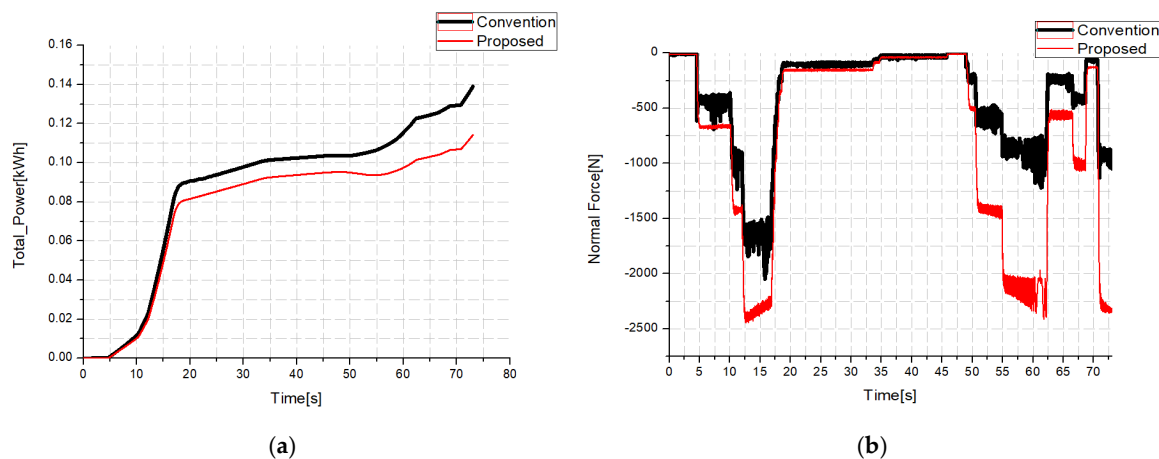
Figure 7. Comparison of existing and proposed condition data: (**a**) Accumulated power consumption and (**b**) Normal train force.

4. Experiment

Figure 8a shows the LIM train of Incheon International Airport in Korea used for the experiment. In order to compare train efficiency, the power system installed on the train and inverter power were directly measured. Figure 8b shows the train's operating route used in the experiment. Five sections were operated over one round trip from Station 101 (the start station) to Station 106 (the end station).
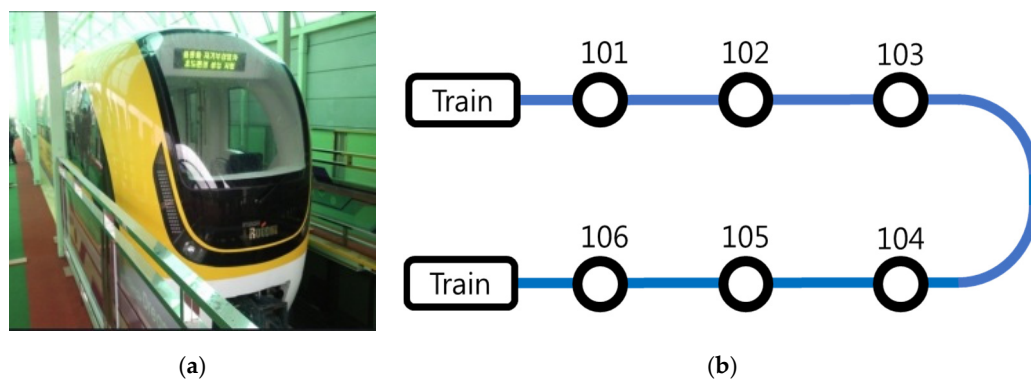

Figure 8. Actual vehicle test conditions and used vehicle: (**a**) Experimental linear induction motor (LIM) and (**b**) Train test-run section.

Table 3 shows the specifications of the trains used in the experiment; the train was composed of 1 car and 2 trains. For comparison, the widely used 13.5 Hz slip-frequency fixed control method and the proposed slip-frequency variable-vector control method were compared. To increase the reliability of the experiment, it was conducted in triplicate, and results were calculated using the average. Lastly, the train was operated using the automatic-train-operation (ATO) method [18], an automatic train control system that propels, rides, and brakes trains according to given commands. The ATO was used for train operations because it reduces the deviation of experiment results using train drivers and quickly responds to slip-frequency fluctuations during operation.

Table 3. Experimental vehicle specifications.

Traction System		Levitation System	
Parameter	**Value**	**Parameter**	**Value**
Length	1785 mm	Length	2600 mm
Number of slots	53	Number of yokes/poles	4
Number of poles	8	Number of coils/poles	2
Air gap	11 mm	Turns/coil	193
Turns/coil	5	Air gap	8 mm
Al plate thickness	5 mm	Pole width	32 mm
Required thrust	60.4 kN	Rated life force	33 kN
Maximal speed	110 km/h		

Figures 9 and 10 show the accumulated power consumption of each part according to actual train operation. Figure 9 shows the operating results from Station 101 to Station 106, and Figure 10 shows the train operating results from Station 106 to Station 101. Figures 9 and 10a show the results of the conventional train control method, and Figures 9 and 10b show those of the proposed control method. In each curve, the green line represents the total amount of consumed power to float the train, the blue line represents the total power consumption used to propel the train, and the red line represents the sum of the power consumption of propulsion. Lastly, the black line indicates the speed of the train. The moment when the curve changed in value was when the train was running between the stations, and the moments when the curve had no value indicate the waiting time after arriving at the station. To exclude the effect of energy consumption caused by differences in waiting times at each station on the results, the consumed energy during the waiting time at each station was removed from the actual comparison. In addition, the test train was used when comparing the actual consumed energy twice as often as the measured value in the two trains.
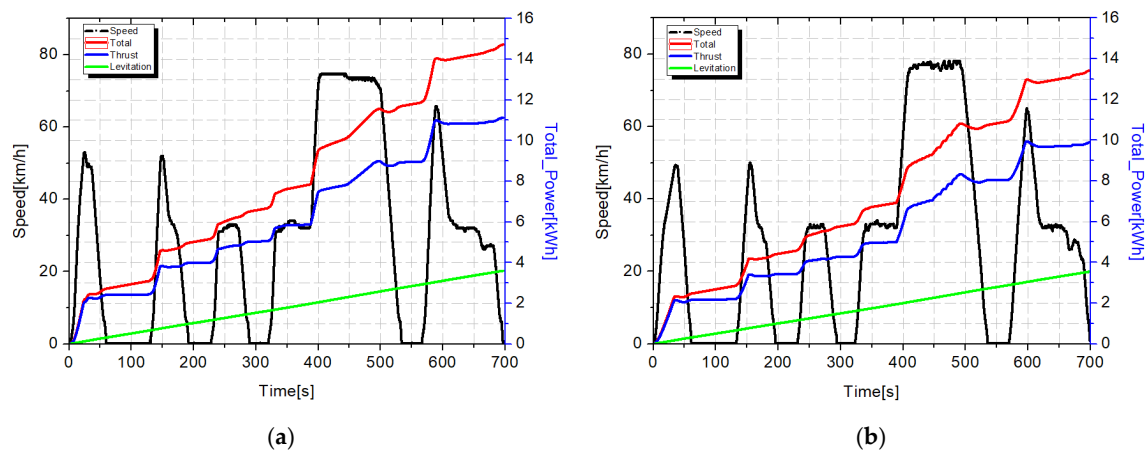

(**a**)

(**b**)

Figure 9. Comparison of accumulated power consumption between existing and proposed methods (101 → 106): (**a**) Conventional method and (**b**) Proposed method.
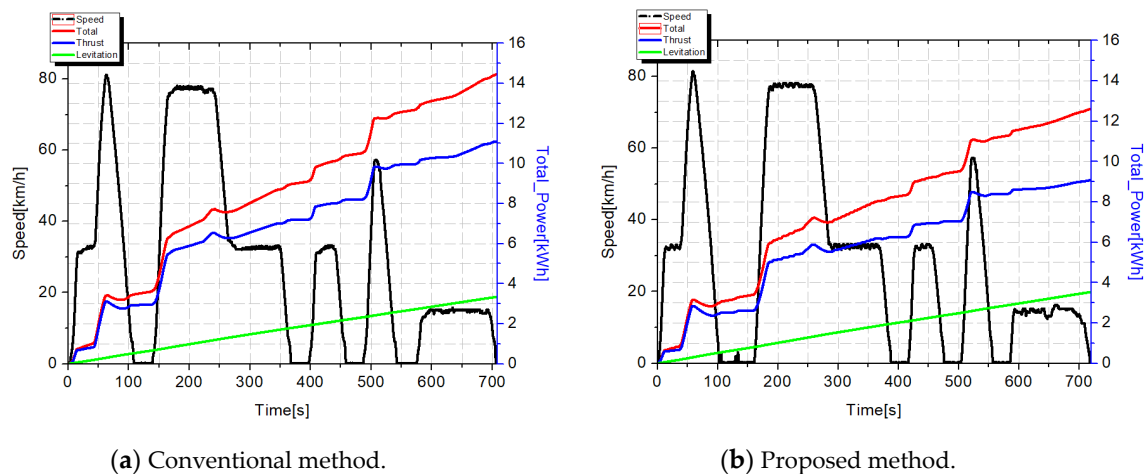
(**a**) Conventional method.　　　　　　　　　　　(**b**) Proposed method.

Figure 10. Comparison of accumulated power consumption of existing and proposed methods (106 → 101): (**a**) Conventional method and (**b**) Proposed method.

Table 4 shows the results of comparing the two methods in consideration of the elimination of reverse waiting time, and (1) quantity and (2) schedule. When moving from Station 101 to Station 106, the total power consumption of the existing method was 27.74 kWh, and the total power consumption of the proposed method was 25.12 kWh. When using the proposed method, there was approximately 2.62 kWh (9.45%) increased efficiency. When moving from Station 106 to Station 101, the total power consumption of the existing method was 27.8 kWh, the total power consumption of the proposed method was 23.64 kWh; when using the proposed method, there was approximately 4.16 kWh (14.96%) increased efficiency. As a result, efficiency increased by approximately 6.78 kWh (12.2%) when using the proposed method, to 55.54 and 48.76 kWh, respectively, from Station 101 to Station 106.

Table 4. Comparison of power-consumption results.

	Operation from 101 to 106		Operation from 106 to 101	
	Conventional	**Proposed**	**Conventional**	**Proposed**
Total (kWh)	27.74	25.12	27.8	23.64
Thrust (kWh)	22.1	19.6	22.1	18.54
Levitation (kWh)	5.64	5.52	5.7	5.1
Reduction rate (%)		9.45%		14.96%

5. Conclusions

In this study, as part of our research on improving the operating efficiency of a maglev train using an LIM, the relationship between train slip frequency, normal force, and propulsion force was analyzed through a mathematical study. Using the analytical results, the slip frequency having the optimal efficiency was derived on the basis of the train's operating conditions while limiting the normal force to the extent to which the levitation system of the train did not fail. Subsequently, slip frequency was changed according to the operating conditions of the train in real time. Through the ATO driving system, a simulation test in which slip frequency was varied on the basis of the driving conditions of the train while it was running, and an experiment using an actual train were conducted. As a result of the simulation test for one operating section in which the actual train was running, when the proposed method was used rather than the existing fixed system slip frequency of 13.5 Hz, a cumulative power-consumption decrease of approximately 24 Wh and an efficiency gain of approximately 17.14% were achieved. These results confirmed that the efficiency improvement using the proposed method was significant. In the case of the experiment, when the proposed method was compared with the existing fixed system slip frequency of 13.5 Hz, the cumulative power consumption decreased by

approximately 6.78 kWh and efficiency increased by approximately 12.2%. Through this, we verified that the proposed method is more efficient than the existing method is (the proposed method uses LIM characteristics, which are suitable for low- and medium-speed types. Therefore, it is difficult to apply to maglev trains with different structures and principles, such as superconducting-repulsion or permanent-magnet types).

Author Contributions: Conceptualization, S.-U.P.; methodology, S.-U.P.; software, H.-U.S.; validation, S.-U.P.; formal analysis, S.-U.P.; investigation, S.-U.P.; resources, J.-W.L.; data curation, S.-U.P.; writing—original-draft preparation, S.-U.P.; writing—review and editing, H.-S.M. and S.-H.O.; visualization, S.-U.P.; supervision, H.-S.M.; project administration, S.-H.O.; funding acquisition, J.-W.L. All authors have read and agreed to the published version of the manuscript.

Conflicts of Interest: The authors declare no conflict of interest.

References

1. Boldea, I.; Nasar, S.A. *Linear Induction Motor. Linear Motion Electromagnetic Devices*; Taylor & Francis: New York, NY, USA, 1997; pp. 35–102.
2. Xu, W.; Zhu, J.G.; Zhang, Y.; Li, Z.; Li, Y.; Wang, Y. Equivalent Circuits for Single-Sided Linear Induction Motors. *IEEE Trans. Ind. Appl.* **2010**, *46*, 2410–2423. [CrossRef]
3. Nozaki, Y.; Yamaguchi, T.; Koseki, T. Equivalent circuit model with parameters depending on secondary speed for high-speed transport—A smart combination of classical modeling and numerical electromagnetic calculation. In Proceedings of the 19th International Conference on Magnetically Levitated Systems Linear Drives, Dresden, Germany, 13–15 September 2006; pp. 537–543.
4. Duncan, J. Linear induction motor-equivalent-circuit model. *IEE Proc. B Electr. Power Appl.* **1983**, *130*, 51–57. [CrossRef]
5. Wang, K.; Li, Y.; Ge, Q.; Shi, L. Indirect field-oriented control of linear induction motor based on optimized slip frequency for traction application. In Proceedings of the 2016 18th European Conference on Power Electronics and Applications, Karlsruhe, Germany, 5–9 September 2016.
6. Lu, C.; Dawson, G.E.; Eastham, T.R. Dynamic performance of a linear induction motor with slip frequency control. In Proceedings of the Canadian Conference on Electrical and Computer Engineering, Vancouver, BC, Canada, 14–17 September 1993.
7. Wallace, A.; Parker, J.; Dawson, G. Slip control for LIM propelled transit vehicles. *IEEE Trans. Magn.* **1980**, *16*, 710–712. [CrossRef]
8. Lu, Q.; Li, Y.; Ye, Y.; Zhu, Z.Q. Investigation of Forces in Linear Induction Motor under Different Slip Frequency for Low-Speed Maglev Application. *IEEE Trans. Energy Convers.* **2013**, *28*, 145–153. [CrossRef]
9. Yang, Z.; Zhao, J.; Zheng, T.Q. A novel traction and normal forces study for the linear induction motor. In Proceedings of the International Conference on Electrical Machines and Systems, Wuhan, China, 17–20 October 2008.
10. Park, S.U.; Zun, C.Y.; Park, D.-Y.; Lim, J.; Mok, H.S. A Study on Improvement of Operation Efficiency of Magnetic Levitation Train Using Linear Induction Motor. *IEEE Trans. Energy Convers.* **2013**, *28*, 145–153. [CrossRef]
11. Ogino, Y.; Murakami, Y.; Nakaoka, M. High performance ultra-low speed control of inverter-fed linear induction motor using vector control scheme. In Proceedings of the IEEE Industry Applications Conference Twenty-Eighth IAS Annual Meeting, Toronto, ON, Canada, 2–8 October 1993.
12. Sung, J.-H.; Nam, K. A new approach to vector control for a linear induction motor considering end effects. In Proceedings of the IEEE Industry Applications Conference. Thirty-Fourth IAS Annual Meeting, Phoenix, AZ, USA, 3–7 October 1999.
13. Kang, G.; Nam, K. Field-oriented control scheme for linear induction motor with the end effect. *IEEE Proc. Electr. Power Appl.* **2005**, *152*, 1565–1572. [CrossRef]
14. Silva, E.F.; Santos, E.B.; Machado, P.C.M.; Oliveria, M.A.A. Vector control for linear induction motor. In Proceedings of the IEEE International Conference on Industrial Technology, Maribor, Slovenia, 10–12 December 2003.

15. Yaohua, L.; Jinqi, R. Drive system of single side linear induction motors. In Proceedings of the International Conference on Electrical Machines and Systems, Wuhan, China, 17–20 October 2008.

16. Wang, K.; Li, Y.; Ge, Q.; Shi, L. An Improved Indirect Field-Oriented Control Scheme for Linear Induction Motor Traction Drives. *IEEE Trans. Ind. Electr.* **2018**, *65*, 9928–9937. [CrossRef]

17. Ooi, B.-T.; White, D. Traction and Normal Forces in the Linear Induction Motor. *IEEE Trans. Power Appl. Syst.* **1970**, *89*, 638–645. [CrossRef]

18. Xiaomin, Z.; Xiang, L. The modeling of test systems of Automatic Train Operation (ATO) in Urban rail transit based on LABVIEW. In Proceedings of the International Conference on Computer Application and System Modeling, Taiyuan, China, 22–24 October 2010.